Responses to Referee #3's comments

We are grateful to the reviewers for their valuable and helpful comments on our manuscript "Mechanistic Insights into Nitric Sulfuric Acid Formation and Its Enhancement of Sulfuric Acid-Ammonia Nucleation under Severe Urban Pollution" (MS No.: **egusphere-2026-3682**). We have revised the manuscript carefully according to reviewers' comments. The point-to-point responses to the Referee #3's comments are summarized below:

Referee Comments:

This manuscript investigated the gas-phase formation mechanism of nitric sulfuric acid (NSA) from the SO_3+ HNO_3 reaction, as well as its subsequent enhancement in sulfuric acid–ammonia nucleation. The results found that NSA is a novel nucleation precursor. The topic is relevant to atmospheric chemistry and the manuscript is generally readable. In my opinion, the present work may be suitable for publication in ACP. However, I note the absence of any discussion regarding field observations of NSA. I also have several comments and suggestions, which follow.

1) Please provide the description of the calculation method for the reactions of SO_3 with HNO_3.

2) In global minimum search step, how did you deal with the calculation results that failed during optimization or that ended up with imaginary frequencies?

3) Where did the authors take the SA-A data from? Or were the clusters recalculated in the present work?

4) Please clarify whether the NSA has determined the most stable structure.

5) Since NA have been detected in the atmosphere of various polluted cities, it would be interesting to see the nucleation rate and cluster growth pathway at ambient conditions more typical to polluted urban environments, that is, higher coagulation sink value, e.g., 2×10^{-2} s^{-1}.

6) In the ACDC simulation, why are the low level energies calculated at M06-2X method used in the input file, rather than high level energies calculated at DLPNO-CCSD(T) method?

7) Figure3. In some cases, the structure obtained from the optimization method may differ from the result of the dual-level calculation; the authors need to explain why the most stable structures obtained at the DLPNO-CCSD(T)/aug-cc-pVTZ//M06-2X/6-311++G(2df,2pd) level were not presented.

8) Line 246, 271-277, missing references.

9) Line 297-298, How is the NSA/SA ratio determined?

10) Figure 1, the figure is unclear and what is the reference state? I think it is sufficient to provide ΔE and there is no need to provide the ICR.

11) Move Figure 2 to SI

12) Figure 4, it is difficult to understand. What do the circles of different sizes represent? It is recommended to provide specific values.

13) Figure 6a, Provide values of flux out.

Response: We would like to thank the reviewer for the positive and valuable comments, and we have revised our manuscript accordingly.

Comment 1.

Please provide the description of the calculation method for the reactions of SO_3 with HNO_3.

Response: We sincerely thank the reviewer for this valuable comment. Following the reviewer's suggestion, the computational details of the SO_3 + HNO_3 reaction have been added to Section 2.1 in Lines 81-88 Page 4 to Lines 89-91 Page 5 of the revised manuscript, which has been reorganized as follows: "To elucidate the gas-phase formation mechanism of NSA via the reaction between SO_3 and HNO_3, quantum chemical calculations were conducted using the Gaussian 09 program (Frisch et al., 2009). The geometries and vibrational frequencies of all stationary points involved in the reaction pathway, including reactants, pre-reactive complexes, transition states (TSs), post-reactive complexes and products, were optimized and characterized at the M06-2X/6-311++G(2*df*,2*pd*) level of theory. The identified TS structures were further validated by intrinsic reaction coordinate (IRC) calculations performed at the same level, confirming the connectivity between the TSs and the corresponding pre-reactive and post-reactive complexes. Subsequently, single-point energy calculations were carried out at the CCSD(T)-F12/cc-pVDZ-F12 level using the ORCA 4.2.0 program (Neese, 2018) to refine the relative energies of the reaction intermediates and pathways.".

Comment 2.

In global minimum search step, how did you deal with the calculation results that failed during optimization or that ended up with imaginary frequencies?

Response: Thank you for this valuable comment. For structures that failed to converge during geometry optimization or exhibited imaginary frequencies, additional verification procedures were applied to ensure the reliability of the final configurations. Initially, non-converged structures were carefully inspected to identify the potential reasons for convergence failure. Depending on the specific causes, the optimization parameters were adjusted and/or the initial geometries were slightly modified, followed by repeated optimization calculations until convergence was achieved. In cases where imaginary frequencies were detected, the corresponding vibrational modes were analyzed in detail to determine the origin of the structural instability. When necessary, the geometries were displaced along the relevant imaginary-frequency modes and subsequently re-optimized. This iterative refinement process was continued until stable local minimum without imaginary frequencies were obtained. Therefore, all structures included in the final global minimum search were confirmed to be fully optimized local minima, ensuring the reliability of the subsequent calculations.

Comment 3.

Where did the authors take the SA-A data from? Or were the clusters recalculated in the present work?

Response: Thank you for this valuable comment. The initial geometry of the SA-A binary cluster was adopted from previous theoretical calculations (***Phys. Chem. Chem. Phys.***, 2018, 20, 17406-17414). To maintain methodological consistency with the computational protocol employed in the present study, the obtained cluster structure was further optimized at the M06-2X/6-311++G(2*df*,2*pd*) level of theory. Subsequently, the relative energy was refined through a high-level single-point calculation using the DLPNO-CCSD(T)/aug-cc-pVDZ method.

Comment 4.

Please clarify whether the NSA has determined the most stable structure.

Response: Thanks for your valuable comments. The NSA structure adopted in this study corresponds to the most stable configuration identified from our calculations. The selection of this structure is justified as follows.

(a) The initial NSA geometry was obtained from the intrinsic reaction coordinate (IRC) calculation of the corresponding transition state as shown in Fig. 1. Specifically, the terminal structure along the IRC pathway was extracted and subsequently used as the starting geometry for further optimization at the M06-2X/6-311++G(2df,2pd) level of theory. The optimized NSA structure was found to be highly consistent with the lowest-energy NSA configuration reported in a previous theoretical study (***J. Am. Chem. Soc.***, 2022, 144, 9172-9177), supporting the reliability of the selected structure.

(b) To independently assess the conformational stability of the adopted NSA structure, a dihedral angle scan was performed by systematically varying the hydrogen atom positions. As shown in Fig. S1, the NSA structure obtained in this study corresponds to the global minimum identified from the dihedral angle scan and agrees well with the most stable conformational arrangement determined from this analysis. These results further confirm that the NSA structure used in the present work represents the most stable configuration.

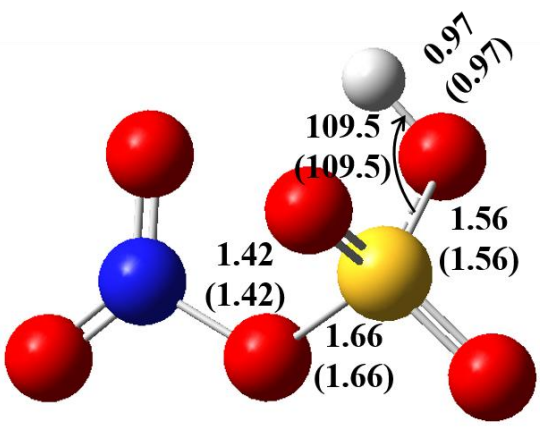


Fig. S1 Optimized the stable geometries of NSA obtained at the M06-2X/6-311++G(2*df*,2*pd*) level of theory from the dihedral angle scan. The values in parentheses denote the corresponding scanned dihedral angles. Bond lengths and angles are given in angstroms (Å) and degrees (°), respectively.

Comment 5.

Since NA have been detected in the atmosphere of various polluted cities, it would be interesting to see the nucleation rate and cluster growth pathway at ambient conditions more typical to polluted urban environments, that is, higher coagulation sink value, e.g., 2×10^{-2} s^{-1}.

Response: Thank you for this valuable suggestion. We appreciate the reviewer's valuable comment. As noted by the reviewer, NA has been observed in the atmosphere of several polluted urban areas, highlighting the importance of evaluating the nucleation rates and cluster growth pathways of NA-containing clusters under conditions representative of polluted environments. In the present study, the coagulation sink (CS) used in the ACDC simulations was set to2×10^{-2} s^{-1}, which corresponds to the relatively high sink conditions typically encountered in polluted urban atmospheres and is consistent with the value suggested by the reviewer. The

applied CS value and its description have been provided in Line 135 on Page 6. Therefore, the nucleation rates and cluster growth pathways reported in this work have been evaluated under a high coagulation sink condition representative of polluted urban environments.

Comment 6.

In the ACDC simulation, why are the low level energies calculated at M06-2X method used in the input file, rather than high level energies calculated at DLPNO-CCSD(T) method?

Response: Thank you for this important comment. We apologize that the description of the computational energy correction procedure was not sufficiently clear in the original manuscript. In the present study, the cluster geometries were optimized at the M06-2X/6-311++G(2*df*,2*pd*) level of theory, and the corresponding electronic energies were subsequently refined by high-level single-point calculations at the DLPNO-CCSD(T)/aug-cc-pVDZ level. The Gibbs free energies employed in the ACDC simulations were obtained by combining the DLPNO-CCSD(T)-corrected electronic energies with the zero-point energy and thermal corrections derived from the M06-2X/6-311++G(2*df*,2*pd*) calculations. Therefore, the thermodynamic parameters used in the ACDC simulations were based on DLPNO-CCSD(T)-refined energies rather than directly using the uncorrected M06-2X energies.

To avoid any potential misunderstanding, the original statement, "Consequently, the 10 most stable structures were refined at the M06-2X/6-311++G(2*df*,2*pd*) level (Elm and Mikkelsen, 2014), and the global minimum was identified based on Gibbs free energy," has been revised in Lines 100-104 on Page 5 of the revised manuscript, which has been organized as "Finally, the 10 lowest-energy structures were further optimized at the M06-2X/6-311++G(2*df*,2*pd*) level (Elm and Mikkelsen, 2014) to identify the isomer with the lowest Gibbs free energy. Based on the optimized geometries, single-point energy calculations were subsequently performed at the DLPNO-CCSD(T)/aug-cc-pVDZ level using the ORCA 4.2.0 program package (Neese, 2018)."

Comment 7.

Figure 3. In some cases, the structure obtained from the optimization method may differ from the result of the dual-level calculation; the authors need to explain why the most stable structures obtained at the DLPNO-CCSD(T)/aug-cc-pVTZ//M06-2X/6-311++G(2*df*,2*pd*) level were not presented.

Response: We appreciate the reviewer's comment. In the present study, the DLPNO-CCSD(T)/aug-cc-pVTZ calculations were performed only as single-point energy calculations using the geometries optimized at the M06-2X/6-311++G(2*df*,2*pd*) level. Therefore, no additional geometry optimization was carried out at the DLPNO-CCSD(T) level. The DLPNO-CCSD(T) method was employed to refine the electronic energies of the M06-2X-optimized structures, whereas the optimized geometries and vibrational frequencies were obtained from the M06-2X/6-311++G(2*df*,2*pd*) calculations. Accordingly, the molecular structures presented in Fig. 3 correspond to the optimized geometries determined at the M06-2X/6-311++G(2*df*,2*pd*) level.

To eliminate potential ambiguity, the original sentence of "Building on these interaction characteristics, Fig. 3 presents the lowest-energy structures of the ternary NSA-SA-A clusters identified from the potential energy surface." has been revised as follows in Lines 224-226 on Page 9 of the revised manuscript, which has

been organized as “Building on these interaction characteristics, Fig. 2 presents the lowest-energy structures of the ternary SA-A-NSA clusters identified at the M06-2X/6-311++G(2*df*,2*pd*) level.”

Comment 8.

Line 246, 271-277, missing references.

Response: Thanks for your valuable comments. We apologize for the missing references in the manuscript. We appreciate the reviewer’s suggestion and agree with this comment. Accordingly, three relevant references have been added at the corresponding locations in the revised manuscript. The specific revisions are as follows:

(a) As for the classical binary nucleation mechanism reported previously, the relevant references have been changed which has been organized as references (Liu et al., 2018).

[1] Liu, L., Li, H., Zhang, H., Zhong, J., Bai, Y., Ge, M., Li, Z., Chen, Y., and Zhang, X.: The role of nitric acid in atmospheric new particle formation, Phys. Chem. Chem. Phys., 20, 17406-17414, https://doi.org/10.1039/C8CP02719F, 2018.

(b) As for the sulfuric acid concentration in the Hyytiälä region, the relevant references have been changed which has been organized as references (Beck et al., 2022).

[1] Beck, L. J., Schobesberger, S., Sipilä, M., Kerminen, V. M., and Kulmala, M.: Estimation of sulfuric acid concentration using ambient ion composition and concentration data obtained with atmospheric pressure interface time-of-flight ion mass spectrometer, Atmos. Meas. Tech., 15, 1957-1965, https://doi.org/10.5194/amt-15-1957-2022, 2022.

(c) As for the sulfuric acid concentration in the western coast of Ireland region, the relevant references have been changed which has been organized as references (Berresheim et al., 2002).

[1] Berresheim, H., Elste T., Tremmel, H. G., Allen, A. G., Hansson, H. C., Rosman, K., Dal Maso, M., Mäkelä, J. M., Kulmala, M., and O'Dowd, C. D.: Gas-aerosol relationships of H_2SO_4, MSA, and OH: Observations in the coastal marine boundary layer at Mace Head, Ireland, J. Geophys. Res., 107, 8100, https://doi.org/10.1029/2000JD000229, 2002.

Comment 9.

Line 297-298, How is the NSA/SA ratio determined?

Response: Thank you for this comment. We apologize for the insufficient clarification regarding the determination of the NSA/SA ratio in the original manuscript. We would like to clarify that the NSA/SA ratios used in the ACDC simulations were not derived from direct atmospheric observations, as quantitative measurements of gas-phase NSA concentrations are currently unavailable. Consequently, the atmospheric abundance of NSA remains poorly constrained. Rather than assigning an observationally derived ratio, we treated the NSA/SA ratio as a prescribed model parameter and varied it over a broad range to investigate how the relative abundance of NSA affects nucleation in comparison with SA.

This type of sensitivity-analysis approach has been adopted in previous studies to assess the potential effects of atmospheric species for which observational constraints are limited (***Atmos. Chem. Phys.***, 2024, 24, 4029-4046; ***Proc. Natl. Acad. Sci. U.S.A.***, 2019, 116, 24966-24971; ***Atmos. Chem. Phys.***, 2026, 26, 3091-3105).

Following this approach, we independently controlled the total concentration of acidic species and their relative contributions in the ACDC simulations. Specifically, the total acid concentration was defined as C_{total} = [NSA] + [SA] and varied from 10^4-10^8 molecules cm^{-3}, while the DMA concentration was fixed at the selected values. For a given C_{total}, the concentrations of NSA and SA were calculated from the prescribed ratio [NSA]/[SA] = *a* : *b*, as follows:

$$[\mathrm{NSA}] = \frac{a}{a+b} C_{total}$$

$$[\mathrm{SA}] = \frac{b}{a+b} C_{total}$$

Five NSA/SA ratios of 1:99, 1:9, 1:1, 9:1, and 99:1 were considered, corresponding to NSA fractions of 1%, 10%, 50%, 90% and 99%, respectively. A pure-SA system with [NSA] = 0 was additionally included as the reference case. These scenarios therefore cover a wide compositional range, from an SA-dominated environment to one increasingly dominated by NSA, allowing the response of the nucleation rate to changes in NSA abundance to be systematically evaluated.

Importantly, the prescribed NSA/SA ratios should not be interpreted as specific atmospheric values or as estimates for any location. Instead, they were introduced solely to provide a controlled sensitivity analysis of the relative roles of NSA and SA in nucleation. Within each simulation series, C_{total} was held constant, whereas the fractional contributions of NSA and SA were varied according to the prescribed ratio. This treatment enables the effect of NSA abundance on the nucleation rate to be evaluated separately from the effect of changes in the total concentration of acidic species.

Comment 10.

Figure 1, the figure is unclear and what is the reference state? I think it is sufficient to provide ΔE and there is no need to provide the ICR.

Response: Thank you for this valuable suggestion. In accordance with the reviewer's recommendation, the IRC calculation has been removed from the revised manuscript. Meanwhile, the potential energy profile calculated at the M06-2X/6-311++G(2*df*,2*pd*) level of theory has been presented in Fig. 1, where the values with and without parentheses correspond to Δ(*E*+ZPE) and ΔH, respectively. The main revision was as follows:

(a) The IRC pathway has been removed from the figure, and the corresponding description of "Fig. 1 presents the intrinsic reaction coordinate pathway for the reaction between SO_3 and HNO_3, accompanied by interaction region indicator (IRI) analysis to elucidate the evolution of atomic interaction strengths along the reaction pathway. Fig. 1 illustrates that the reaction follows a mechanism consisting of two successive steps. At the first stage of the reaction, the appearance of a blue region on the IRI isosurface between SO_3 and HNO_3 indicates the formation of a weakly bound $SO_3\cdots HNO_3$ reactant complex (a). This complex adopts a six-membered ring configuration, exhibiting a stabilization energy of 6.70 kcal·mol^{-1}, in close agreement with the previously reported value of 6.94 kcal·mol^{-1} (Long et al., 2022). As the system evolves along the reaction coordinate, the blue region on the isosurface becomes more pronounced, reflecting a gradual strengthening of the attractive interaction. Subsequently, the reaction crosses transition state (c) with an associated energy barrier

of 3.61 kcal·mol^{-1}, comparable to the value of 3.75 kcal·mol^{-1} reported by Long et al (Long et al., 2022). Concurrently, the original O4-H bond progressively weakens, while a new bond forms between the O6 atom of HNO_3 and the S atom of SO_3. At the final stage of the reaction, the IRI isosurface is dominated by a large green region, indicating the generation of a stable nitric sulfuric acid (O_2NOSO_3H, NSA) characterized by typical covalent bond features." has also been deleted from the revised manuscript.

(b) In the revised Fig. 1, the potential energy profile of the gas-phase reaction has been incorporated, where the values with and without parentheses correspond to Δ(*E*+ZPE) and ΔH, respectively.

(c) The description of the gas-phase reaction mechanism has been reorganized as "As illustrated in Fig. 1, the gas-phase reaction of SO_3 with HNO_3 involves the sequential formation of a pre-reactive complex and its subsequent transformation into NSA. Initially, the two reactants associate through the O3-H and S-O6 interactions, yielding a stable six-membered-ring $SO_3\cdots HNO_3$ complex. This complex is stabilized by 6.90 kcal·mol^{-1}, in close agreement with the previously reported stabilization energy of 6.94 kcal·mol^{-1} (Long et al., 2022). As the reaction evolves toward the transition state, the O3-H and S-O6 distances decrease to 1.22 and 2.55 Å, respectively, while the original O4-H bond becomes progressively weakened. At the transition state, the weakening of the O4-H bond is accompanied by the development of a new S-O6 bond between the SO_3 and HNO_3 moieties, thereby facilitating the subsequent formation of NSA. The calculated activation barrier is 3.90 kcal·mol^{-1}, which is in close agreement with the previously reported value of 3.80 kcal·mol^{-1} (Long et al., 2022). The consistency between these barrier heights supports the reliability of the calculated reaction pathway." in Lines 141-145 Page 6 to Lines 146-152 Page 7 of the revised manuscript.

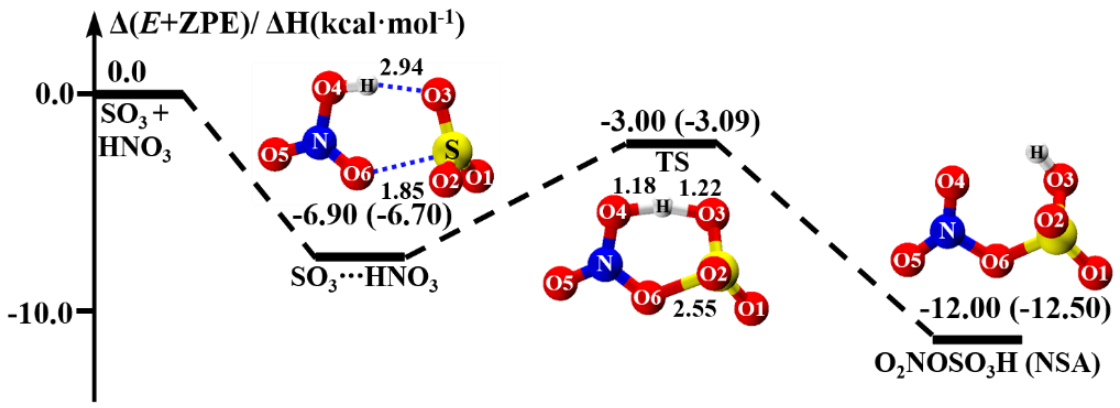


Fig. 1 Schematic potential energy profile of the gas-phase $SO_3 + HNO_3 \rightarrow O_2NOSO_3H$ reaction. Bond distances are given in angstroms and were optimized at the M06-2X/6-311++G(2*df*,2*pd*) level. The corresponding energies were obtained at the CCSD(T)-F12/cc-pVDZ-F12//M06-2X/6-311++G(2*df*,2*pd*) level. Values in parentheses denote Δ(*E*+ZPE), whereas those without parentheses represent ΔH.

Comment 11.

Move Figure 2 to SI.

Response: Thanks for your valuable comments. Following the reviewer's suggestion, Fig. 2 was moved to the supplementary material, which was labeled as Fig. S5.

Comment 12.

Figure 4, it is difficult to understand. What do the circles of different sizes represent? It is recommended to provide specific values.

Response: Thank you for this valuable suggestion. We apologize for the ambiguity in the original presentation of Fig. 4. The circles were intentionally drawn with different sizes to distinguish clusters of different sizes, with larger circles representing larger clusters. The corresponding Gibbs formation free energies of the individual clusters are provided in Table S7 on page S21 of the Supporting Information. To clarify the graphical representation, we have revised the caption of Fig. 4 accordingly: "**Fig. 3** Gibbs formation free energies (ΔG, kcal·mol^{-1}) of $a_m b_n$ clusters (a = acid ($(NSA)_x(SA)_y$), b = base (A), $0 \le n \le m \le 3$, $0 \le x \le m$, $0 \le y \le m$, and $x + y = m$ at 278.15 K at the DLPNO-CCSD(T)/aug-cc-pVTZ//M06-2X/6-311++G(2*df*,2*pd*) level of theory; The circles of different sizes indicate the sizes of the corresponding clusters." The revised caption has been incorporated into Lines 261-263 on Page 11 of the revised manuscript.

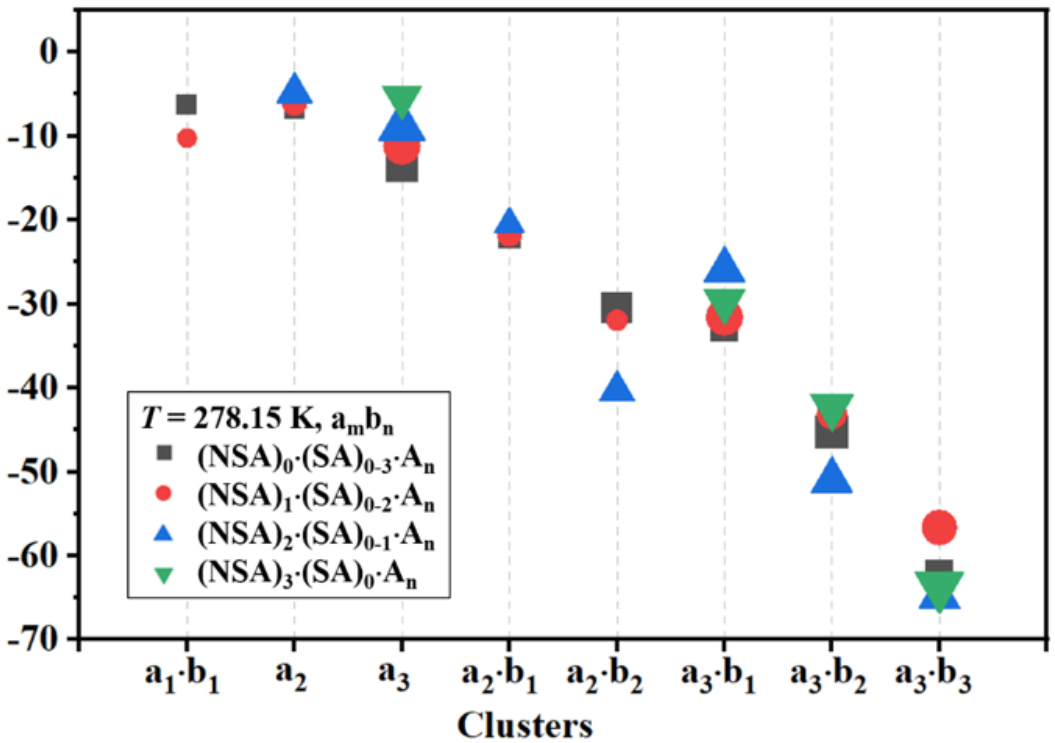


Fig. 3 Gibbs formation free energies (ΔG, kcal·mol^{-1}) of $a_m b_n$ clusters (a = acid ($(NSA)_x(SA)_y$), b = base (A), $0 \le n \le m \le 3$, $0 \le x \le m$, $0 \le y \le m$, and $x + y = m$ at 278.15 K at the DLPNO-CCSD(T)/aug-cc-pVTZ//M06-2X/6-311++G(2*df*,2*pd*) level of theory; The circles of different sizes indicate the sizes of the corresponding clusters.

Comment 13.

Figure 6a, Provide values of flux out.

Response: Thanks for your valuable comments. For reviewers' comments, we have added the specific flux-out values to Fig. 5(a) in the revised manuscript. The revised Fig. 5(a) is shown below.

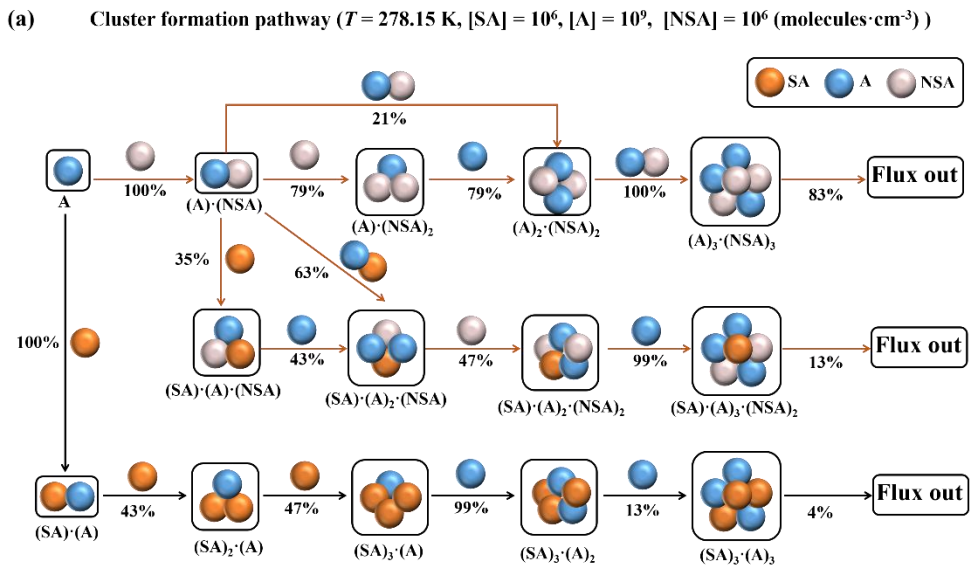


Fig. 5 Nucleation mechanism of the SA-A-NSA system. (a) Cluster formation pathway at T = 278.15 K under [SA] = 10^6 molecules·cm^{-3}, [A] = 10^9 molecules·cm^{-3} and [NSA] = 10^6 molecules·cm^{-3}.